ROYAL SOCIETY OF CHEMISTRY

PAPER

Check for updates

Conductive ionogel for the study of charge transport through SAM-based junctions in aqueous solution†

Xiyue Bai, Ningyue Chen, Zhou Cao and Yuan Li (iD) *

The urgency of the application of large-area molecular junctions in aqueous environments has garnered significant attention, driven by the necessity for biomolecular testing under physiological conditions and the monitoring of chemical reactions in solution. In this study, we synthesized a conductive ionogel as a top electrode to measure the electrical properties of self-assembled monolayers (SAMs). The SAMs for the test have different terminal groups, including −COOH, −CH_3 and −F, exhibiting distinct affinities with water molecules. The variation in current density for each SAM can be attributed to the amount of water molecules between the electrode and SAMs. The electrical tests conducted in buffer solutions indicate that our tunneling process is dominated by electrons rather than ions, laying the foundation for testing biomolecules in physiological environments. We utilized ionogel electrodes for testing molecular junctions based on myoglobin and conducted temperature-dependent experiments with excellent repeatability. The exploration of ionogel electrodes contributes to our ability to conduct more complex measurements like rapid testing or drug screening, particularly in aqueous environments.

1. Introduction

The integration of wet chemistry with single-molecule electrical measurements has successfully demonstrated its efficacy in the investigation of intricate charge transport through molecules surrounded by liquid molecules.[1–4] Yet, most of the studies are achieved by single-molecule break junctions.[5] In order to advance this technology further, there is a need for stable junctions that can offer capabilities in structural customization,[6] sensing of reactions,[7] and mechanical flexibility in flexible electronic applications.[8] Measurements of current densities across junctions having the SAMs (self-assembled monolayers) as the transport medium, have been proven to be a promising platform for creating stable molecular junctions and fabricating devices with high integration potential.[9–11] Conducting charge transport measurements through SAMs with the junction immersed in an aqueous solution has the potential to open up a range of intriguing studies related to biomaterials and bioactivities.[12,13] These studies could include investigations into processes such as molecular docking systems,[14] bio-relevant systems,[15] and the behavior of fully hydrated proteins or enzymes.[16]

The interaction of dipoles at the interface plays a crucial role in various fields such as perovskite,[17] lithium-ion batteries,[18] and polymer materials.[19] In molecular junctions, dipoles affect the efficiency of tunneling transport or the work function of electrodes. Douglas Natelson *et al.* observed a linear vibrational Stark effect due to the permanent electric dipole moment.[20] Takhee Lee *et al.* reported photo-responsive molecular junctions enhanced by different intrinsic dipole moments.[21] The dipole interaction in a liquid environment could also influence the measured tunneling current by the STM break junction technique.[22–24]

This paper demonstrates that the charge transport measurements under different aqueous solutions can, to a certain extent, recognize molecule-originated transport signals and be applied to studying the charge transport through fully hydrated proteins. We fabricate and characterize a polymer-based ionogel-carbon black (IG–CB) electrode further by measuring the electrical properties of molecular junctions in different environments and the ultimate conditions for application to understand the dipole interaction in molecular junctions with liquid environments. This design can be potentially applied to understanding weak interactions or chemical reactions happening at the surface of SAMs in liquid environments.

By single-molecule junctions, there are numerous demonstrations about the electrical characterization and chemical reaction conducted in solution environments.[25–29] For example, Murakoshi *et al.* reported the *in situ* observations of geometrical and electronic structural dynamics using mechanically controllable

Key Laboratory of Organic Optoelectronics and Molecular Engineering, Department of Chemistry, Tsinghua University, Beijing 100084, China. E-mail: yuanli_thu@tsinghua.edu.cn

This journal is © The Royal Society of Chemistry 2024

J. Mater. Chem. C, 2024, **12**, 481–488 | **481**

break junctions in aqueous solutions.[30] Luo *et al.* measured the temperature-dependent conductance of single-molecule junctions in aqueous solutions and observed the thermal motion of water molecules.[31] Measuring the conductance of molecular junctions in aqueous solution is the foundation for research and technology in bioelectronics. For instance, Guo *et al.* showed the distinguishment of four amino acids and their enantiomers using patterned graphene electrodes chemically connected with molecules, and therefore amino acid identification and single-molecule protein sequencing became possible by high throughput electrical measurements.[32] Similarly, the recognition of carbohydrate epimers can be achieved *via* the current fluctuations reported by the group of Zhang.[33] The development of single-molecule junctions in aqueous solutions is very successful, but on the other hand, SAM-based junctions in solution progress slowly.

As for the SAM-based junctions, mercury is used as the material of top electrodes for solid-state junctions as well as for junctions in liquid.[34] However, due to the toxicity of mercury, eutectic gallium–indium (EGaIn) was developed and the properties of this non-Newtonian fluid are highly suitable for the measurement of molecular junctions, generating highly reproducible data.[35] In subsequent studies, researchers have employed various materials for the top electrical contacts of SAMs, such as gold nanowires,[36] PEDOT:PSS,[37] graphene,[38] gold nanoparticles.[39] However, research is focused on the solid-state junctions or devices, and very few cases investigated the charge transport in solution. Whitesides *et al.* developed EGaIn junctions in organic solvents and found that the efficiency of charge transport is related to external environments of organic solvents due to the formation of thin liquid films between EGaIn and SAMs.[40] Using conducting atomic force microscopy (C-AFM), S. J. O'Shea *et al.* found that the charge transports across a *n*-decanethiol SAM in nonpolar liquids strongly alter the mechanical response to the AFM tip.[41] Besides, H. D. Abruña *et al.* reported that it is common for the solution environment to influence the charge transport of SAMs, which does not occur through direct contact between two electrodes.[42] The obstacle of developing SAM-based junctions in aqueous solution is to find a proper top electrode to softly contact with SAMs as well as capable of being used in water to investigate the dipole interaction and apply into bioelectronic measurements.

In our previous work, we have developed a new type of ionogel electrode that has been proven to have excellent stability to be the top electrode both in air and pure water environments and the ability to measure the activation energy of protein junctions as the temperature changes.[43] In this study, we explore our studies to give more choices of aqueous solutions from water to two typical buffer solutions: 0.01 M phosphate buffer saline (PBS) and 0.01 M tris(hydroxymethyl)aminomethane hydrochloride (Tris) buffer solution. We chose three different SAMs with very similar chain length (same number of CH_2 units) but with different terminal groups, which are –COOH, –CH_3 and –F, respectively. Those three terminal groups yielding different hydrophobicity on the surface enable us to investigate whether there will be liquid

layers in between the SAMs and top electrodes. We alter the applied voltage to the junctions under different conditions (air, water, and buffers) to give the proper voltage that can be used for measurements. Finally, we showcase the repeatability of the IG–CB electrode for measuring the activation energy of protein junctions. In this work, we find that the affinity strength between the liquid environment and SAM can have an impact on the electron transport with the IG–CB electrode, and the charge carriers, in our IG–CB electrode system, participating in the process of charge transport in buffer are electrons instead of the ions. The mechanism of charge transport in aqueous solution depends on the structure of the molecules in SAMs, which is similar with the experiments in air with EGaIn.

2. Experimental section

2.1. Materials

1-Ethyl-3-methyl imidazolium bis(trifluoromethylsulfonyl)imide ($[C_2mim][NTf_2]$) (97%) and poly(ethylene glycol) diacrylate (MW = 400) were purchased from Meryer (Shanghai) Chemical Technology Co., Ltd. 1-Hydroxycyclohexyl phenyl ketone (98%) was purchased from Zhengzhou City Erqi district Kecheng chemical products firm. Ethyl acrylate (99%) and 10-bromodecanoic acid (97%) were purchased from Energy Chemical. Carbon black (Black Pearls 2000) (99.99%) was purchased from Cabot Corporation. $1H,1H,2H,2H$-perfluorodecanethiol (97+%) was purchased from Zancheng (Tianjin) Technology Co., Ltd. 1-Decanethiol (99.5%) was purchased from Shanghai Aladdin Biochemical Technology Co., Ltd. 1× phosphate buffer saline (PBS) solution (99%) was purchased from Adamas life. 1 M tris(hydroxymethyl)aminomethane hydrochloride (Tris) solution (99.9%) was purchased from Beijing i-presci Scientific Technology Co., Ltd. 11-Mercaptoundecanoic acid (95%) was purchased from Shanghai Macklin Biochemical Technology Co., Ltd. Myoglobin (95–100%) was purchased from Shanghai yuanye Bio-Technology Co., Ltd. Other compounds mentioned in this study were synthesized by ourselves and the synthesis procedures are given in the ESI† (Fig. S1 and S2).

2.2. Fabrication of the IG–CB electrode

We mixed ethyl acrylate (0.1 mL, 0.92 mmol) with the ionic liquid of $[C_2mim][NTf_2]$ (0.92 mL), poly(ethylene glycol)diacrylate (0.0022 g, 5.52 μmol) and 1-hydroxycyclohexyl phenyl ketone (7.00 mol%, 0.0132 g, 64.4 μmol), which was exposed under UV light for one hour. To increase the conductivity of the material, we ground the carbon black with ionogel with the weight percentage of 15% for it is a balance between the roughness and conductance. We constructed a mold using a poly(dimethylsiloxane) (PDMS) polymer sheet, which was subsequently filled with IG–CB electrode material. To prepare the PDMS mixture, we added a curing agent at a concentration of 10 wt%. Next, the mixture was transferred into an oven and cured at 80 °C for a duration of 1 hour. Once the curing process was completed, the PDMS material was cut into square sheets measuring 1.0 cm × 1.0 cm. Then we used a PDMS puncher to

482 | *J. Mater. Chem. C*, 2024, **12**, 481–488

This journal is © The Royal Society of Chemistry 2024

create 36 holes in each sheet, each with a diameter of 1.0 mm. These holes were then filled with IG–CB material. The PDMS sheet containing IG–CB-filled holes was placed on a smooth silicon wafer positioned on a heated table with the surface heated to 80 °C. The PDMS sheet was pressed against the silicon wafer for 30 seconds to ensure the flatness of the IG–CB at the bottom of each hole. This process finally yielded a top electrode with IG–CB material.

2.3. Preparation of samples

We prepared the template-stripped Au or Ag surfaces following the procedure previously reported.[44] The RMS of Au is 0.410 nm and Ag is 0.333 nm (Fig. S3, ESI†). Subsequently, we detached the Au^{TS} or Ag^{TS} (TS = template stripped) substrates from the silicon wafer and immersed them in 1.0 mM ethanolic solutions of SC$_9$COOH, SC$_{10}$ or SC$_{10}$F for a duration of 3 hours at room temperature. Then, we subjected the substrates to a gentle ethanol rinse and dried them under a stream of nitrogen gas.

For the protein junction, we fabricated the SAMs of SC$_{10}$COOH in the same way. Next, we immersed the SAMs into the myoglobin solution with 1.0 mg mL^{-1} for a period of 30 minutes. The protein samples underwent a water rinse immediately before the junction measurements.

2.4. The formation of junctions

First, we fabricated each molecular junction in a cell with a square of prominence in the middle, where the chip was placed on and a tungsten needle was stabbed upon the chip. Next, we added the liquid solutions into the cell until the liquid level is covered with the chip. The IG–CB electrode was positioned on the top surface of the SAMs. The tungsten needle and the IG–CB electrode are electrically connected to a sourcemeter. For

different choices of SAMs and solutions, we prepared the junctions from the first step.

3. Results and discussion

3.1. Characterization of IG–CB

The process of IG–CB synthesis is facile only with the operation of UV light and grinding as shown in Fig. 1a and the Experimental section. The ionogel based on [C$_2$mim][NTf$_2$] shows strong conductivity due to the addition of carbon black, which changes the charge carriers from ions to electrons and improves the efficiency of charge transport significantly. We manually punched 36 holes filled with IG–CB in a 1 × 1 cm^2 area, which can yield 36 junctions at the same time (Fig. 1b) with very good flexibility (Fig. 1c). We tried our best to achieve a relatively smooth surface of IG–CB with the RMS roughness of 6.269 nm shown in Fig. 1d by the method of AFM as before.[43] We used ultraviolet photoelectron spectroscopy (UPS) to measure the work function of the IG–CB surface to be 4.8 eV as previously reported[43] which is comparable to the work function of polycrystalline Ag (4.7–4.8 eV) and Au (5.0–5.2 eV) (Fig. S4, ESI†).

3.2. Electrical properties of aqueous solution tested by IG–CB top electrodes

We begin our discussion with the interaction between different SAMs and aqueous solution, as shown in Fig. 2a. These SAMs exhibit three distinct terminal groups: –COOH, –CH$_3$, –F (see the structures in Fig. S5, ESI†). The total number of carbons of the three molecules is ten with a film thickness estimated around 1.0 nm, and it is a relatively largely studied chain length in molecular junctions. We do not observe a clear odd–even effect of the current density from our junctions.
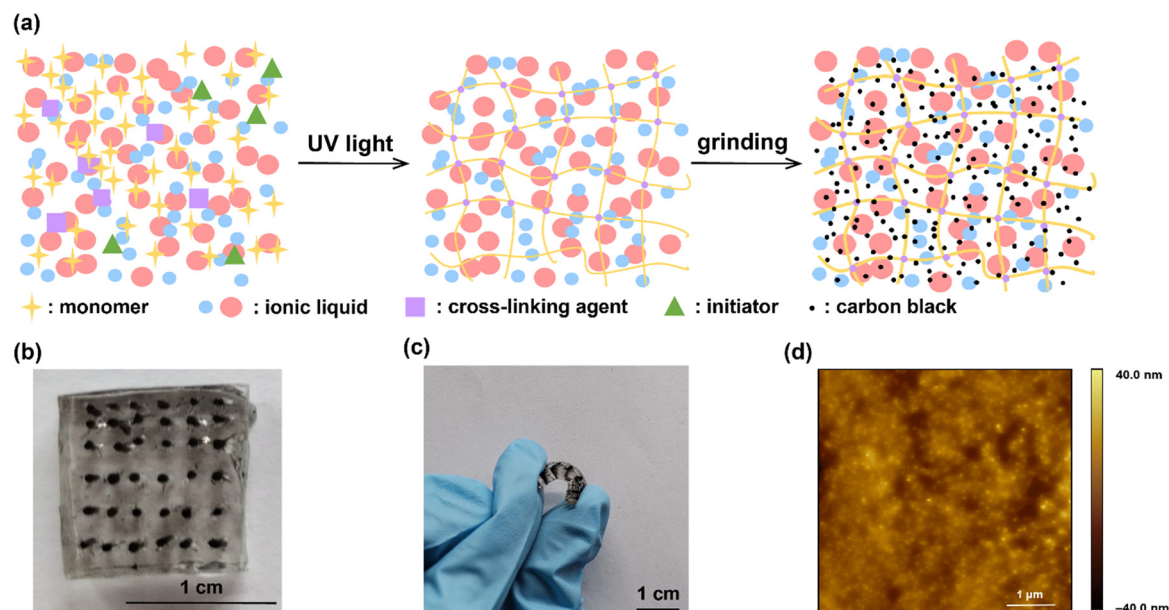

Fig. 1 (a) The schematic illustrations of the synthesis process. (b) The device of the IG–CB electrode. (c) Photograph of the electrode device bent by fingers. (d) The AFM image of IG–CB.
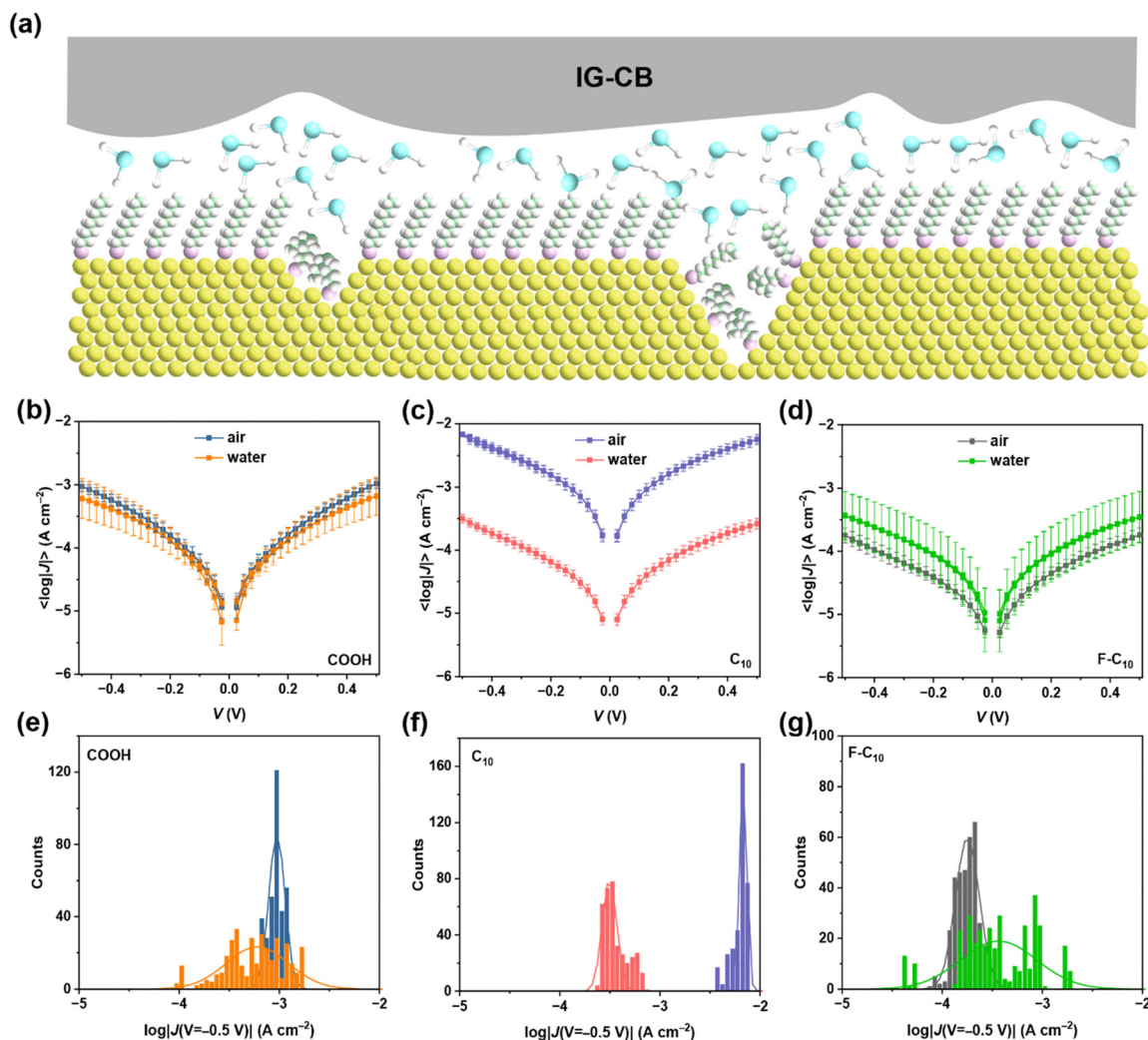
Fig. 2 (a) The scheme of molecular junctions conducted in water. (b) Plots of the $\langle\log|J(V)|\rangle$ curves for $Au^{TS}–SC_9COOH//IG–CB$ junctions tested in air and water. (c) Plots of the $\langle\log|J(V)|\rangle$ curves for $Au^{TS}–SC_{10}//IG–CB$ junctions tested in air and water. (d) Plots of the $\langle\log|J(V)|\rangle$ curves for $Au^{TS}–SC_{10}F//$ IG–CB junctions tested in air and water. (e)–(g) The corresponding histograms of $\log|J|$ at -0.5 V with Gaussian fits.

Among these SAMs, SC_9COOH demonstrates the highest affinity towards aqueous solutions, while $SC_{10}F$ shows the least. Our investigation focuses on measuring the charge transport of diverse SAMs within aqueous solutions, revealing the potential of IG–CB as an electrode material for solution-based reactions. Fig. 2b–d shows the stable J–V curves and each sample has a 100% yield, as shown in Table 1. In the measuring process, we applied ±0.50 V between the bottom electrode and the IG–CB electrode with the step size of 0.025 V and the scan rate of 140 mV s^{-1}, recording 360 scans for each SAM. The maximum voltage range that the IG–CB electrode can withstand is ±6.0 V in air and ±1.5 V in aqueous solution (Fig. S6, ESI†), which is the safe bias window, limited by the electrochemical window of the ionogel matrix.[45] We have examined the reproducibility and stability of our transport data and we can safely conclude that the migration of carbon black inside the electrode is unlikely to happen, rendering it suitable for prolonged and stable utilization.[43] We speculate that the difference between current density in air and water arises from the affinity of the SAMs and

liquid environment. We find that the SAMs of SC_{10} in the presence of water result in dramatic decreases in current densities, where the water layer tends to pile up on the surface of SC_{10} rather than on the surface of –F or –COOH terminated groups. The current densities of SC_9COOH and $SC_{10}F$ in water and in air are statistically overlapped.

The SAMs of SC_9COOH can adsorb water molecules both in air and water, resulting in a similar and relatively small current density. Conversely, SAMs of SC_{10} can capture the water layers in aqueous solution while the moisture content in air is insufficient for it, which elucidates the pronounced disparities in current density between the two states. In the case of $SC_{10}F$, similar to SC_{10}, it can allow neither vapor nor water to immerse between SAMs and the electrode, leading to the overlapped current density. However, the SAMs of $SC_{10}F$ present a weak coupling with the top electrode in air, which accounts for the elevated current density observed in air compared to water. These findings show that the efficiency of electron transport depends on the distance of tunneling, which is impacted by the

484 | J. Mater. Chem. C, 2024, **12**, 481–488

This journal is © The Royal Society of Chemistry 2024

Table 1 The statistical results of every junction

Molecule	Environment	Scan rate (mV s^{-1})	Number of junctions	Number of shorts	Voltage range (V)	Step size	Number of traces	Yield (%)
SC$_9$COOH	Solid	140	15	0	±0.5	0.025	360	100
SC$_{10}$	Solid	140	15	0	±0.5	0.025	360	100
SC$_{10}$F	Solid	140	15	0	±0.5	0.025	360	100
SC$_9$COOH	Water	140	15	0	±0.5	0.025	360	100
SC$_{10}$	Water	140	15	0	±0.5	0.025	360	100
SC$_{10}$F	Water	140	15	0	±0.5	0.025	360	100
SC$_9$COOH	PBS	140	15	0	±0.5	0.025	360	100
SC$_{10}$	PBS	140	15	0	±0.5	0.025	360	100
SC$_{10}$F	PBS	140	15	0	±0.5	0.025	360	100
SC$_9$COOH	Tris	140	15	0	±0.5	0.025	360	100
SC$_{10}$	Tris	140	15	0	±0.5	0.025	360	100
SC$_{10}$F	Tris	140	15	0	±0.5	0.025	360	100
SC$_9$COOH	PBS	50	15	0	±0.5	0.025	360	100
SC$_{10}$	PBS	50	15	0	±0.5	0.025	360	100
SC$_{10}$F	PBS	50	15	0	±0.5	0.025	360	100
SC$_9$COOH	PBS	100	15	0	±0.5	0.025	360	100
SC$_{10}$	PBS	100	15	0	±0.5	0.025	360	100
SC$_{10}$F	PBS	100	15	0	±0.5	0.025	360	100
SC$_9$COOH	PBS	200	15	0	±0.5	0.025	360	100
SC$_{10}$	PBS	200	15	0	±0.5	0.025	360	100
SC$_{10}$F	PBS	200	15	0	±0.5	0.025	360	100
SC$_9$COOH	Tris	50	15	0	±0.5	0.025	360	100
SC$_{10}$	Tris	50	15	0	±0.5	0.025	360	100
SC$_{10}$F	Tris	50	15	0	±0.5	0.025	360	100
SC$_9$COOH	Tris	100	15	0	±0.5	0.025	360	100
SC$_{10}$	Tris	100	15	0	±0.5	0.025	360	100
SC$_{10}$F	Tris	100	15	0	±0.5	0.025	360	100
SC$_9$COOH	Tris	200	15	0	±0.5	0.025	360	100
SC$_{10}$	Tris	200	15	0	±0.5	0.025	360	100
SC$_{10}$F	Tris	200	15	0	±0.5	0.025	360	100
−COOH//Mb	Solid	140	15	0	±1.0	0.05	360	100
−COOH//Mb	Water	140	15	0	±1.0	0.05	360	100
−COOH//Mb each temperature	Water	140	1	0	±1.0	0.05	10	100

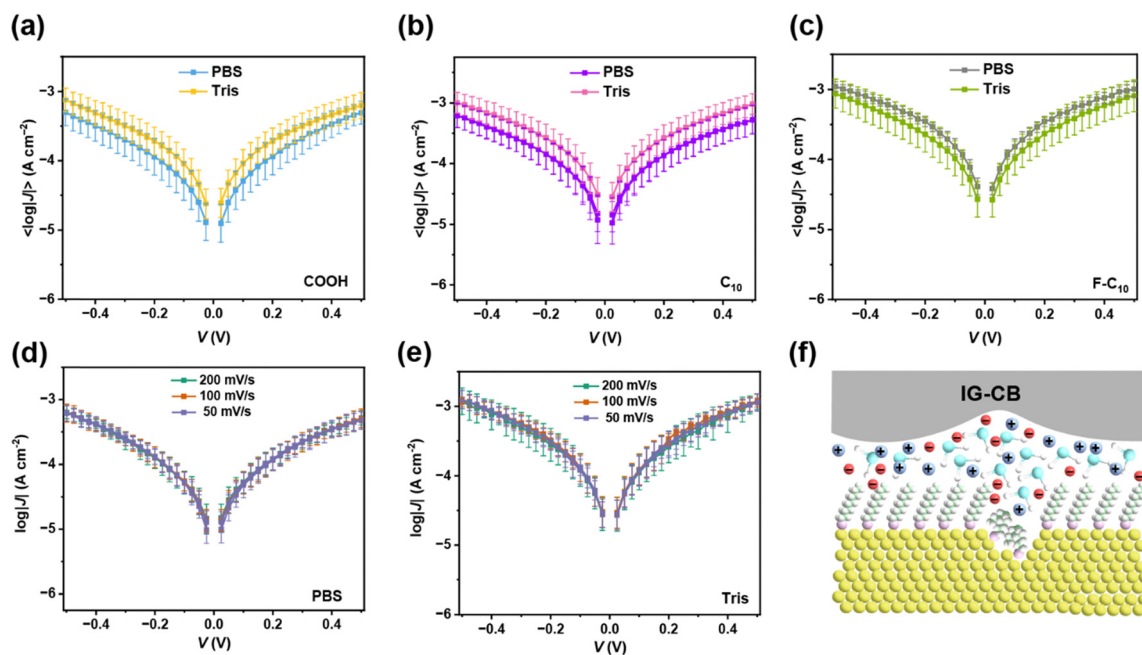**Fig. 3** (a) Plots of the ⟨log|$J(V)$|⟩ curves for Au^{TS}−SC$_9$COOH//IG−CB junctions tested in PBS and Tris buffer. (b) Plots of the ⟨log|$J(V)$|⟩ curves for Au^{TS}−SC$_{10}$//IG−CB junctions tested in PBS and Tris buffer. (c) Plots of the ⟨log|$J(V)$|⟩ curves for Au^{TS}−SC$_{10}$F//IG−CB junctions tested in PBS and Tris buffer. (d) Plots of the ⟨log|$J(V)$|⟩ curves for Au^{TS}−SC$_{10}$//IG−CB junctions tested in PBS with different scan rates. (e) Plots of the ⟨log|$J(V)$|⟩ curves for Au^{TS}−SC$_{10}$//IG−CB junctions tested in Tris with different scan rates. (f) The scheme of molecular junctions conducted in buffer.
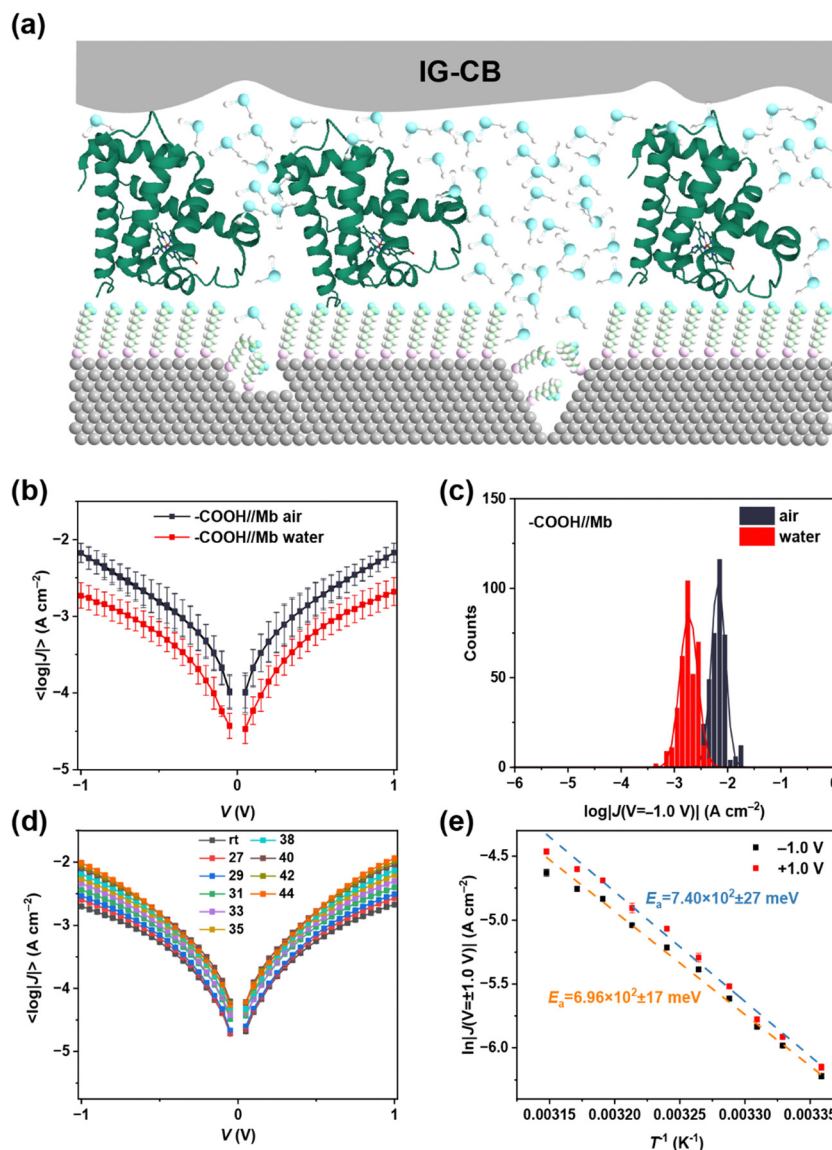
Fig. 4 (a) The scheme of molecular junctions with myoglobin proteins conducted in water. (b) Plots of the ⟨log|J(V)|⟩ curves for Ag^{TS}-SC$_{10}$COOH//Mb//IG−CB junctions tested in air and water. (c) The corresponding histograms of log|J| at −1.0 V with Gaussian fits. (d) T-dependent ⟨log|J(V)|⟩ data for the junctions of Ag^{TS}-SC$_{10}$COOH//Mb//IG−CB in water. (e) Corresponding Arrhenius plots for ⟨ln|J|⟩ at ±1.0 V.

number of water layers captured by the surface of the measurements. Furthermore, it's noteworthy that the Gaussian distribution of SAMs in water is broader than in air in Fig. 2e–g, as a phenomenon potentially attributed to the thermal motion of water molecules.[46,47] The presence of water molecules between the electrode and SAM is uncertain, and the number of water layers is also undetermined, which contributes to a broader distribution of current density in water.

In addition to the pure water, buffer is also an important environment of measurement especially for biomolecules or other biorelevant events. Fig. 3a–c reveals the results of ⟨log|J(V)|⟩ curves in buffer solutions, demonstrating similar interactions between SAMs and the two kinds of buffer solutions. The scan rate dependent measurements shown in Fig. 3d and e indicate that the charge carriers through SAMs are

electrons not free ions. Although the ions in buffer are abundant enough to participate under such a strong electrical field (Fig. 3f), the highly ordered and densely packed SAMs blocked the possibility of ion transport and electrons can be directly transported through the SAMs *via* the direct contact between the bottom and top electrodes. The stability of our junctions lays a robust foundation for application to more complicated systems of monolayers of fully hydrated proteins.

3.3. Temperature-dependent measurement of charge transport through proteins

In Fig. 4, we showcase the protein junction measurements with IG−CB as a suitable electrode in water. We employed nonspecific adsorption of myoglobin (Mb) on top of the surface of SC$_{10}$COOH SAMs *via* electrostatic interactions (Fig. 4a),

486 | J. Mater. Chem. C, 2024, 12, 481–488

This journal is © The Royal Society of Chemistry 2024

which can preserve the structure and function of proteins on metallic electrodes. The junction measurements shown in Fig. 4b and c are similar to our previous studies of cytochrome C by IG–CB electrodes.[43] One of the most prominent advantages of the IG–CB electrode is to measure the activation energy of the protein junction in its native status, that is in physiologically relevant solutions. Fig. 4d and e show temperature-dependent experiments in aqueous solution with myoglobin protein junctions. To determine the activation energy of Mb under ± 1.0 V, we measured the Ag^{TS}-$SC_{10}COOH$//Mb//IG–CB junctions from room temperature (about 25 °C) to 44 °C, and plotted the $\langle \ln|J| \rangle$ as a function of $1/T$ with Arrhenius fits. This is a very reliable measurement where similar values of activation energy can be acquired from three completely independent experiments (Fig. S7, ESI†). The small fluctuations of the $\langle \ln|J| \rangle$ in Fig. 4e may arise from factors such as the random orientation of adsorbed Mb, the surface roughness of the IG–CB electrodes and the error of the temperature control, but these have negligible impacts on the values of the activation energy that we measured.

4. Conclusions

In conclusion, we have demonstrated a new type of conductive ionogel as a suitable material to be a choice of top electrode for SAM-based junctions when the measurement conditions require water environments or even buffers. We conducted a comprehensive measurement for the charge transport properties of SAMs with different terminal groups in various environments, which indicates the capacity of IG–CB to test in water. The disparity in current density not only reflects the interaction between SAMs and the electrode, but also provides insights into the amount of water at the interface. The nature of charge carriers in aqueous solutions is electrons instead of ions proven by rate-dependent experiments. The results from junctions in buffer solutions and measured with proteins show the potential of the IG–CB electrode for bioelectrical experiments at molecular level incorporation with SAMs. Our findings pave the way for future developments in large-area molecular junctions for studies on the electron transport and tunneling mechanism of biological molecules and solution reactions.

Conflicts of interest

There are no conflicts to declare.

Acknowledgements

References

1 E. M. Dief, P. J. Low, I. Diez-Perez and N. Darwish, *Nat. Chem.*, 2023, **15**, 600–614.

2 C. Huang, A. V. Rudnev, W. Hong and T. Wandlowski, *Chem. Soc. Rev.*, 2015, **44**, 889–901.

3 X. Xie, P. Li, Y. Xu, L. Zhou, Y. Yan, L. Xie, C. Jia and X. Guo, *ACS Nano*, 2022, **16**, 3476–3505.

4 J. Bai, X. Li, Z. Zhu, Y. Zheng and W. Hong, *Adv. Mater.*, 2021, **33**, 2005883.

5 I. Stone, R. L. Starr, Y. Zang, C. Nuckolls, M. L. Steigerwald, T. H. Lambert, X. Roy and L. Venkataraman, *Nat. Rev. Chem.*, 2021, **5**, 695–710.

6 C. Tang, X.-L. Jiang, S. Chen, W. Hong, J. Li and H. Xia, *J. Am. Chem. Soc.*, 2023, **145**, 10404–10410.

7 H. Chen, C. Jia, X. Zhu, C. Yang, X. Guo and J. F. Stoddart, *Nat. Rev. Mater.*, 2023, **8**, 165–185.

8 A. M. Najarian, B. Szeto, U. M. Tefashe and R. L. McCreery, *ACS Nano*, 2016, **10**, 8918–8928.

9 P. A. Van Hal, E. C. P. Smits, T. C. T. Geuns, H. B. Akkerman, B. C. De Brito, S. Perissinotto, G. Lanzani, A. J. Kronemeijer, V. Geskin, J. Cornil, P. W. M. Blom, B. De Boer and D. M. De Leeuw, *Nat. Nanotechnol.*, 2008, **3**, 749–754.

10 H. Jeong, D. Kim, D. Xiang and T. Lee, *ACS Nano*, 2017, **11**, 6511–6548.

11 S. Song, B. Cho, T. W. Kim, Y. Ji, M. Jo, G. Wang, M. Choe, Y. H. Kahng, H. Hwang and T. Lee, *Adv. Mater.*, 2010, **22**, 5048–5052.

12 A. Shaver, S. D. Curtis and N. Arroyo-Curras, *ACS Appl. Mater. Interfaces*, 2020, **12**, 11214–11223.

13 R. E. McGovern, S. C. Feifel, F. Lisdat and P. B. Crowley, *Angew. Chem., Int. Ed.*, 2015, **54**, 6356–6359.

14 C. W. Fuller, P. S. Padayatti, H. Abderrahim, L. Adamiak, N. Alagar, N. Ananthapadmanabhan, J. Baek, S. Chinni, C. Choi, K. J. Delaney, R. Dubielzig, J. Frkanec, C. Garcia, C. Gardner, D. Gebhardt, T. Geiser, Z. Gutierrez, D. A. Hall, A. P. Hodges, G. Hou, S. Jain, T. Jones, R. Lobaton, Z. Majzik, A. Marte, P. Mohan, P. Mola, II, P. Mudondo, J. Mullinix, N. Thuan, F. Ollinger, S. Orr, Y. Ouyang, P. Pan, N. Park, D. Porras, K. Prabhu, C. Reese, T. Ruel, T. Sauerbrey, J. R. Sawyer, P. Sinha, J. Tu, A. G. Venkatesh, S. VijayKumar, L. Zheng, S. Jin, J. M. Tour, G. M. Church, P. W. Mola and B. Merriman, *Proc. Natl. Acad. Sci. U. S. A.*, 2022, **119**, e2112812119.

15 X. Huang, J. Chen, X. Fang, C. Yan and H. Shao, *J. Electroanal. Chem.*, 2019, **837**, 143–150.

16 C. E. Nordgren, D. J. Tobias, M. L. Klein and J. K. Blasie, *Biophys. J.*, 2002, **83**, 2906–2917.

17 Y. Zhao, B. Yang, Q. Wu, Y. Zhou, F. Guo and S. Zhao, *Nanoscale*, 2021, **13**, 16226–16233.

18 K. Wen, C. Xin, S. Guan, X. Wu, S. He, C. Xue, S. Liu, Y. Shen, L. Li and C.-W. Nan, *Adv. Mater.*, 2022, **34**, 2202143.

19 Z. Cheng, W. Feng, Y. Zhang, L. Sun, Y. Liu, L. Chen and C. Wang, *Adv. Mater.*, 2023, **35**, 2301005.

20 Y. Li, P. Zolotavin, P. Doak, L. Kronik, J. B. Neaton and D. Natelson, *Nano Lett.*, 2016, **16**, 1104–1109.

This journal is © The Royal Society of Chemistry 2024

J. Mater. Chem. C, 2024, **12**, 481–488 | **487**

21 C. Lee, J. Kim, J. Lee, W. Lee, M. Song, K.-Y. Baek, J. Shin, J. Nam, J. Lee, K. Kang and T. Lee, *Adv. Opt. Mater.*, 2022, **10**, 2200049.

22 L. Xiang, P. Zhang, C. Liu, X. He, H. B. Li, Y. Li, Z. Wang, J. Hihath, S. H. Kim, D. N. Beratan and N. Tao, *Matter*, 2020, **3**, 166–179.

23 B. Capozzi, J. Xia, O. Adak, E. J. Dell, Z.-F. Liu, J. C. Taylor, J. B. Neaton, L. M. Campos and L. Venkataraman, *Nat. Nanotechnol.*, 2015, **10**, 522–527.

24 M. Kotiuga, P. Darancet, C. R. Arroyo, L. Venkataraman and J. B. Neaton, *Nano Lett.*, 2015, **15**, 4498–4503.

25 Y. Zang, Q. Zou, T. Fu, F. Ng, B. Fowler, J. Yang, H. Li, M. L. Steigerwald, C. Nuckolls and L. Venkataraman, *Nat. Commun.*, 2019, **10**, 4482.

26 C. Tang, T. Stuyver, T. Lu, J. Liu, Y. Ye, T. Gao, L. Lin, J. Zheng, W. Liu, J. Shi, S. Shaik, H. Xia and W. Hong, *Nat. Commun.*, 2023, **14**, 3657.

27 C. Yang, Y. Li, S. Zhou, Y. Guo, C. Jia, Z. Liu, K. N. N. Houk, Y. Dubi and X. Guo, *Nat. Chem.*, 2023, **15**, 972–979.

28 R. Sha, L. Xiang, C. Liu, A. Balaeff, Y. Zhang, P. Zhang, Y. Li, D. N. Beratan, N. Tao and N. C. Seeman, *Nat. Nanotechnol.*, 2018, **13**, 316–321.

29 A. C. Aragones, N. L. Haworth, N. Darwish, S. Ciampi, N. J. Bloomfield, G. G. Wallace, I. Diez-Perez and M. L. Coote, *Nature*, 2016, **531**, 88–91.

30 T. Konishi, M. Kiguchi, M. Takase, F. Nagasawa, H. Nabika, K. Ikeda, K. Uosaki, K. Ueno, H. Misawa and K. Murakoshi, *J. Am. Chem. Soc.*, 2013, **135**, 1009–1014.

31 H. Cao, J. Jiang, J. Ma and Y. Luo, *J. Am. Chem. Soc.*, 2008, **130**, 6674–6675.

32 Z. Liu, X. Li, H. Masai, X. Huang, S. Tsuda, J. Terao, J. Yang and X. Guo, *Sci. Adv.*, 2021, **7**, eabe4365.

33 J. Im, S. Biswas, H. Liu, Y. Zhao, S. Sen, S. Biswas, B. Ashcroft, C. Borges, X. Wang, S. Lindsay and P. Zhang, *Nat. Commun.*, 2016, **7**, 13868.

34 A. O. Solak, S. Ranganathan, T. Itoh and R. L. McCreery, *Electrochem. Solid-State Lett.*, 2002, **5**, E43–E46.

35 R. C. Chiechi, E. A. Weiss, M. D. Dickey and G. M. Whitesides, *Angew. Chem., Int. Ed.*, 2008, **47**, 142–144.

36 X. Yu, R. Lovrincic, L. Sepunaru, W. Li, A. Vilan, I. Pecht, M. Sheves and D. Cahen, *ACS Nano*, 2015, **9**, 9955–9963.

37 G. Wang, S.-I. Na, T.-W. Kim, Y. Kim, S. Park and T. Lee, *Org. Electron.*, 2012, **13**, 771–777.

38 G. Wang, Y. Kim, M. Choe, T.-W. Kim and T. Lee, *Adv. Mater.*, 2011, **23**, 755–760.

39 D. Kos, G. Di Martino, A. Boehmke, B. de Nijs, D. Berta, T. Foldes, S. Sangtarash, E. Rosta, H. Sadeghi and J. J. Baumberg, *Nat. Commun.*, 2020, **11**, 5905.

40 Y. Li, S. E. Root, L. Belding, J. Park, H. J. Yoon, C. Huang, M. Baghbanzadeh and G. M. Whitesides, *J. Phys. Chem. B*, 2023, **127**, 407–424.

41 N. N. Gosvami, S. K. Sinha, M. P. Srinivasan and S. J. O'Shea, *J. Phys. Chem. C*, 2008, **112**, 297–302.

42 D. Acevedo and H. D. Abruna, *J. Phys. Chem.*, 1991, **95**, 9590–9594.

43 X. Bai, P. Li, W. Peng, N. Chen, J.-L. Lin and Y. Li, *Adv. Mater.*, 2023, **35**, 2300663.

44 L. Yuan, N. Nerngchamnong, L. Cao, H. Hamoudi, E. del Barco, M. Roemer, R. K. Sriramula, D. Thompson and C. A. Nijhuis, *Nat. Commun.*, 2015, **6**, 6324.

45 A. M. O'Mahony, D. S. Silvester, L. Aldous, C. Hardacre and R. G. Compton, *J. Chem. Eng. Data*, 2008, **53**, 2884–2891.

46 A. A. Higazy, M. E. Kassem and M. B. Sayed, *J. Phys. Chem. Solids*, 1992, **53**, 549–554.

47 T. Y. Chen and P. F. Luckham, *J. Phys. D: Appl. Phys.*, 1994, **27**, 1556–1563.